INTERNATIONAL JOURNAL FOR NUMERICAL METHODS IN FLUIDS
Int. J. Numer. Meth. Fluids 2004; **44**:1045–1061 (DOI: 10.1002/fld.689)

Multigrid simulations of detached shock waves

P. Gerlinger*,† and M. Aigner

Institut für Verbrennungstechnik der Luft- und Raumfahrt, Universität Stuttgart, Germany

SUMMARY

The use of multigrid convergence acceleration techniques is investigated for supersonic and hypersonic flows over blunt bodies. In these cases detached shock waves occur that usually complicate convergence for multigrid methods. It is shown that a simple damping of the restricted residual error enables convergence without the application of expensive upwind restriction or prolongation operators. The achieved reduction in CPU time increases with increasing free stream Mach number. A similar technique may be used for reactive flows where the restricted residual error is damped in regions of high chemical activity. A spherical nose projectile moving at Mach 6.46 in a stochiometric hydrogen–air mixture serves as a test case to demonstrate the efficiency of this approach in case of combustion. Copyright © 2004 John Wiley & Sons, Ltd.

KEY WORDS: multigrid; supersonic flow; turbulence; combustion; detached shock waves

1. INTRODUCTION

Multigrid techniques belong to the most efficient numerical methods for solving large fluid flow problems. During the last years research is underway to realize multigrid methods that achieve *text book multigrid efficiency* (TME) for realistic problems. Brandt [1] has defined TME as an optimally convergent method achieving fully converged solutions for the discretized set of equations in less than 10 multigrid cycles. An optimal method would achieve convergence with arithmetic operations that scale according to $O(N)$, where N ($N=N_V m$) is the number of volumes (N_V) multiplied with the number of equations (m) to be solved in every volume. For purely elliptic problems, TME has already been achieved. For hyperbolic systems like the incompressible Euler equations $O(N)$ methods have also been realized [2, 3] as well as $O(Nm^2)$ solvers for the compressible Navier–Stokes equations [4]. Some of the techniques developed distinguish between elliptic and hyperbolic factors of the system and treat them appropriately [5]. However, up to now most results presented are for simple geometries and still lack practical aspects as turbulence modelling and highly stretched grids

*Correspondence to: P. Gerlinger, Institut für Verbrennungstechnik, DLR VT, Pfaffenwaldring 38-40, Stuttgart 70569, Germany.
†E-mail: peter.gerlinger@dlr.de

Contract/grant sponsor: Deutsche Forschungsgemeinschaft (DFG); contract/grant number: SFB 259

Received 27 December 2002
Revised 22 October 2003

required in near wall regions. Moreover, TME is not attained for solutions of the compressible Reynolds-averaged Navier–Stokes equations in general. While most applications concerning TME deal with aerodynamic airfoil or simple channel flows, such solvers are also required for complex internal flows with jet injection, swirl and recirculation. However, there is hope that grid independent $O(N)$ methods for general applications will be developed in the next years.

Another probably at least equally demanding problem for multigrid methods is the simulation of reacting flows based on finite-rate chemistry. Due to the strong non-linearity of the chemical source terms, the similarity between the coarse and fine grid solution gets lost in most cases that may cause divergence [6, 7]. Even if the solver is able to damp out high frequency error components, the question remains how to deal with the strong non-linear chemistry source terms at coarse grid levels. Because of their strongly non-linear form and because they describe a physical local process, recalculation usually fails at least for more than two grid levels. Especially, multigrid simulations of detached flames still are a great challenge. Moreover, in case of turbulent combustion and assumed pdf (probability density function) modelling the second moment equations (e.g. variance of energy and variance species fluctuations) contain stiff chemical source terms too that have to be treated by the multigrid method [8]. On the other hand, convergence acceleration is especially needed for such simulations due to the large set of governing equations and therefore long CPU times.

For most of the basic problems of standard multigrid methods to achieve convergence (strong shock waves in supersonic and hypersonic flows, highly stretched grids, turbulence and chemical source terms) there are simple remedies. However, some of these techniques reduce the theoretically achievable convergence acceleration and convergence rates are still grid-dependent. On the other hand, most of these techniques are easy to implement into the existing codes, they are robust and reduce the CPU times by factors between 2 and 10 even for complex flows with large density ratios (in case of hydrogen injections) and combustion [8].

In this paper the full approximation storage (FAS) scheme of Brandt [9, 10] is the basis for the multigrid method used. A version for implicit approximately factored schemes is employed which was first presented by Jameson and Yoon [11]. The good damping properties of the implicit LU-SGS algorithm allow multigrid convergence even for cell aspect ratios up to 10 000 [12]. The modifications introduced to enable convergence in case of strong shock waves is a simple damping of the restricted residual error [13]. A similar treatment is used for chemical reactions where the restricted residuals are damped in regions of high chemical activity [7, 8]. As to deal with non-linear source terms of the low Reynolds number q-ω turbulence closure used, non-linear contributions based on spatial derivatives are transfered to coarse grid levels without recalculation and are kept frozen [13]. For non-reactive flows these techniques worked very stable and reliably for a great variety of different applications. In case of combustion the proposed method has proven to achieve considerable accelerations for attached hydrogen and methane flames but it is still test case and grid size dependent if detached flames are simulated.

This paper investigates the application of the mentioned multigrid method to the simulation of detached shock waves, both with and without combustion. In contrast to attached shocks where the shock position is defined by the geometry this is not the case for detached shock waves. If slightly different shock positions are obtained at different grid levels this may cause problems for the multigrid solver [14]. A similar situation arises in case of detached flames

where the flame position is defined by the calculated ignition delay which may differ between different grid levels. It will be shown that the proposed techniques enable convergence and that the achieved acceleration slightly increases with increasing inflow Mach number. The investigated non-reactive test cases cover the range from Mach 2 to 8, the reactive test case has a Mach number of 6.46.

2. FLUID EQUATIONS AND NUMERICAL SCHEME

For the investigation of high-speed flows with combustion, the expanded time-averaged Navier–Stokes equations are solved which are given in two-dimensional form by

$$\frac{\partial \mathbf{Q}}{\partial t} + \frac{\partial(\mathbf{F}_j - \mathbf{F}_{vj})}{\partial x_j} = \mathbf{S}, \quad j = 1, 2 \tag{1}$$

$\mathbf{Q}$ denotes the conservative variable vector

$$\mathbf{Q} = [\rho, \rho u_1, \rho u_2, \rho E, \rho q, \rho \omega, \rho Y_\alpha]^{\mathrm{T}}, \quad \alpha = 1, 2, \ldots, N_k - 1 \tag{2}$$

$\mathbf{F}_j$ are inviscid, and $\mathbf{F}_{vj}$ are viscous flux vectors in x_j direction, respectively. The source vector $\mathbf{S}$ results from turbulence and chemistry. The variables in Equation (2) are the density ρ, velocity components u_j, the total specific energy E, the turbulence variables $q = \sqrt{k}$ (k = turbulent kinetic energy), and $\omega = \varepsilon/k$ (ε = dissipation rate of k), and the species mass fractions Y_α. N_k is the number of different species. A two-equation low Reynolds number q-ω turbulence model was chosen as turbulence closure [15, 13]. The source vector appearing on the right-hand side of Equation (1) is given by

$$\mathbf{S} = [0, 0, 0, 0, S_q, S_\omega, S_\alpha]^{\mathrm{T}}, \quad \alpha = 1, 2, \ldots, N_k - 1 \tag{3}$$

where S_q and S_ω are source terms of the q-ω turbulence model, and S_α are species source terms resulting from chemistry. The unsteady form of the governing equations is integrated in time using an implicit finite-volume LU-SGS algorithm [11, 16, 13]. The numerical finite-volume solver is first order in time and second order in space. Inviscid and viscous fluxes are discretized by central differences. A second- and fourth-order matrix dissipation allows a good shock capturing with low numerical dissipation [17].

3. THE MULTIGRID METHOD

For non-linear problems there are two possibilities to apply multigrid methods: The first one is a global linearization of the problem, e.g. by a Newton method and subsequent application of a multigrid method for linear problems to the linearized set of equations. However, the more important and more frequently used approach is to apply the multigrid method directly to the non-linear problem being called FAS scheme by Brandt [5, 9]. This technique is used throughout this paper in a version for implicit approximately factored schemes [11, 13]. First, we want to describe the procedure of the standard FAS multigrid method before modifications are introduced, necessary to simulate detached shock waves.

For all simulations to follow a full coarsening is used. That means that a coarser grid is formed by eliminating every other grid line on the previous finer mesh. In this way a hierarchy of up to four levels $k=1,2,3,4$ is created. The multigrid cycle may be started on the finest or coarsest grid (nested multigrid). Here, a V-cycle with only 1 coarse grid iteration is employed without post relaxations during prolongation. No benefit was obtained from additional coarse grid smoothings. One smoothing step of the implicit LU-algorithm may symbolically be expressed by

$$\mathrm{LU}(\mathbf{Q}^k)\Delta\mathbf{Q}^k=\mathbf{R}(\mathbf{Q}^k) \tag{4}$$

where LU is the implicit operator, $\mathbf{R}$ the residual, k indicates the level of the grid, and $\Delta\mathbf{Q}^k$ is the correction obtained from one LU-sweep. After one relaxation sweep is performed on the finest level, the FAS V-cycle strategy is as follows:

Step 1: The present fine grid solution and the recalculated residuals are transferred from the finest to the next coarser grid by

$$\mathbf{Q}_0^{k+1}=r_k^{k+1}\mathbf{Q}^k, \qquad \mathbf{R}_\mathrm{c}^{k+1}=\bar{r}_k^{k+1}\mathbf{R}(\mathbf{Q}^k) \tag{5}$$

where the subscripts 0 and c are standing for the initialized coarse grid solution and the collected residuals, respectively. The restriction operators r_k^{k+1} for the transfer of the variable vector from fine to coarse grids is given by

$$r_k^{k+1}\mathbf{Q}^k=\frac{1}{\Omega^{k+1}}\sum_{l=1}^{4}\Omega_l^k\mathbf{Q}_l^k \tag{6}$$

where Ω are the corresponding cell areas. In this paper a full coarsening is used and always four fine grid volumes are collected forming one coarse grid volume. The residuals $\mathbf{R}$ (and later also $\mathbf{T}$) are therefore restricted by

$$\bar{r}_k^{k+1}\mathbf{R}^k=\sum_{l=1}^{4}\mathbf{R}_l^k \text{ for } k=1, \quad \bar{r}_k^{k+1}\mathbf{T}^k=\sum_{l=1}^{4}\mathbf{T}_l^k \text{ for } k>1 \tag{7}$$

using a simple adding up of four fine grid values.

Step 2: According to Jameson and Yoon [11] a forcing function is defined by

$$\mathbf{P}^{k+1}=\mathbf{R}_\mathrm{c}^{k+1}-\mathbf{R}(\mathbf{Q}_0^{k+1}) \quad \text{for } k=1 \tag{8}$$

which is the difference between the transferred residuals from the fine grid and the recalculated coarse grid residuals for which the transferred variables $\mathbf{Q}_0^{k+1}$ are used. The driving residual error for the coarse grid iteration is the sum of the forcing function and the calculated residual

$$\mathbf{T}^{k+1}=\mathbf{R}(\mathbf{Q}^{k+1})+\mathbf{P}^{k+1} \tag{9}$$

Step 3: The coarse grid solution is updated by

$$\mathrm{LU}(\mathbf{Q}^{k+1})\Delta\mathbf{Q}^{k+1}=\mathbf{T}^{k+1} \tag{10}$$

Steps 1–3 are repeated successively until the coarsest grid level is reached. However, the forcing function for $k>1$ is now calculated by

$$\mathbf{P}^{k+1}=\bar{r}_k^{k+1}\mathbf{T}(\mathbf{Q}^k)-\mathbf{R}(\mathbf{Q}_0^{k+1}) \tag{11}$$

instead of Equation (8).

Step 4: Finally, the coarse grid corrections obtained are prolongated back to the finer grids by

$$\mathbf{Q}^k_{\text{new}} = \mathbf{Q}^k + p^k_{k+1}(\mathbf{Q}^{k+1}_{\text{new}} - \mathbf{Q}^{k+1}_0) \tag{12}$$

where p^k_{k+1} is a prolongation operator for the transfer from coarse to fine grids. A bilinear interpolation is used in the present case. The boundary conditions are treated in the same way at all grid levels.

3.1. Modifications of standard multigrid methods

While standard multigrid techniques work stable and highly efficient in case of elliptic sets of equations, problems arise if supersonic or hypersonic flows have to be treated. Reduced multigrid efficiencies or even failure are observed in case of

- sets of governing equations which are of mixed types (e.g. elliptic hyperbolic),
- *grid alignment* (main flow direction aligns with one co-ordinate direction),
- strong attached or detached shock waves,
- turbulence closures that include strong non-linear source terms (especially low Reynolds number versions),
- chemically reacting flows simulated with finite-rate chemistry,
- highly stretched grids to resolve near wall layers.

Unfortunately, at least in case of high-speed combustion several of these points appear at the same time. For a part of these problems there are already reliable techniques to get multigrid methods working but an $O(Nm^2)$ method for combustion is still not available.

3.1.1. Shock waves. The hyperbolic character of the set of governing equations in supersonic and hypersonic flows usually causes divergence of standard multigrid methods if strong shock waves occur. Standard restriction and prolongation operators do not account for the limited regions of influence in case of supersonic flows. Thus non-physical upwind influence are possible that, especially near shock waves, may avoid convergence. Different approaches have been introduced to enable multigrid convergence in such cases. A complex and computational expensive method that has been tested for the Euler equations is based on characteristic restriction and prolongation operators [18]. Another upwind restriction and prolongation technique for the Euler equations was presented by Koren and Hemker [14]. A very simple non-characteristic upwind prolongation is used in Reference [12] for the simulation of viscous high-speed mixing. Ferm and Lötstedt [19] identified oscillatory error components at shock waves to be responsible for bad convergence rates. As a consequence, they introduced a residual-dependent restriction operator. For simple model test cases and the Euler equations strong improvements are reported with this technique for two grid levels. A simple and robust working method is a damping of the restricted residual error in the vicinity of shock waves [20, 7, 12, 13]. Shock waves are always associated with strong pressure gradients that may be localized by

$$v^{\xi}_{i,j} = \frac{|p_{i+1,j} - 2p_{i,j} + p_{i-1,j}|}{(1-\chi)(|p_{i+1,j} - p_{i,j}| + |p_{i,j} - p_{i-1,j}|) + \chi(p_{i+1,j} + 2p_{i,j} + p_{i-1,j})} \tag{13}$$

A similar formulation is used for the η direction. The parameter χ defines the smoothness of this sensor as well as its activation in case of weak disturbances. Usually $\chi = 0.5$ is used. To locate regions where the transferred residuals should be reduced the shock sensors in ξ and η direction are combined

$$\kappa_{i,j}^k = C^k \max(\nu_{i,j}^{\xi}, \nu_{i-1,j}^{\xi}, \nu_{i+1,j}^{\xi}, \nu_{i,j}^{\eta}, \nu_{i,j-1}^{\eta}, \nu_{i,j+1}^{\eta}) \tag{14}$$

and Equation (7) is replaced by

$$\bar{r}_k^{k+1}\mathbf{R}^k = \sum_{l=1}^{4} \mathbf{R}_l^k \max(0, 1 - \kappa_l^k), \qquad \bar{r}_k^{k+1}\mathbf{T}^k = \sum_{l=1}^{4} \mathbf{T}_l^k \max(0, 1 - \kappa_l^k) \tag{15}$$

The maximum in these equations is only required if values $C^k > 1$ are chosen. This method has proven to work extremely stable for attached shock waves and is investigated for the simulation of detached shocks in this paper. If bow shocks in front of a blunt body occur, an additional problem is that the exact shock position is defined from aerodynamic reasons. In that case a shift between the coarse and fine grid shock position may cause divergence. Thus the damping of the restricted residual error has to cover the spatial regions of fine and coarse grid shock waves.

3.1.2. Non-linear source terms of turbulence closures. For the hypersonic test cases investigated turbulence is of minor importance. There is only a weak production of turbulence intensity directly at the shock waves. Therefore, the multigrid modifications of turbulent production rates at coarse grid levels are not of importance for this paper. A stable and robust simulation of turbulent test cases even with low Reynolds number turbulence closures is possible if parts of strongly non-linear source term contributions are treated frozen at coarse grid levels. A detailed description of this technique may be found in Reference [13].

3.1.3. Non-linear source terms due to chemistry. A more severe problem than turbulence source terms are the chemical production rates in case of finite-rate chemistry. Due to the strong non-linearity of these terms they have to be treated implicitly. The question that arises is how such non-linear terms are treated at the coarse grid levels. A simple recalculation as well as a freezing as in case of turbulence usually causes failure of the multigrid method. The reason for divergence in case of freezing is the much stronger coupling between the variable vector and source terms in case of chemistry. One possibility to achieve multigrid convergence that works quite stable at least for attached flames is a damping of the restricted residual error in regions of high chemical activity [7, 8]. This is associated with losses in the theoretical possible acceleration but stabilizes the multigrid simulation. In some simulations the coarse grid time step additionally has to be reduced in the same regions [8]. This is especially required in case of implicit solvers. To locate regions of high chemical activity an additional sensor

$$\gamma^k = B^k \left(\frac{1}{N_k} \sum_{i=1}^{N_k} \frac{|S_i^k|}{S_{i,\max}^k + \varepsilon} \right)^{\alpha} \tag{16}$$

is needed. $S_{i,\max}^k$ is the maximum absolute production rate of species i within the flowfield, B^k is a grid level dependent constant ($0 \leqslant B^k \leqslant 1$) and ε is a small number to avoid division by

zero. This sensor is limited to $0 \leqslant \gamma \leqslant 1$. An exponent α of 0.3 ensures a smooth distribution. Thus in case of combustion the restriction operators of Equation (15) are replaced by

$$\bar{r}_k^{k+1}\mathbf{R}^k = \sum_{l=1}^{4} \mathbf{R}_l^k \max[0, \min(1-\kappa_l^k, 1-\gamma_l^k)]$$

$$\bar{r}_k^{k+1}\mathbf{T}^k = \sum_{l=1}^{4} \mathbf{T}_l^k \max[0, \min(1-\kappa_l^k, 1-\gamma_l^k)] \tag{17}$$

Because combustion is always associated with density gradients, the use of a density-based sensor instead of Equation (16) is possible too. If the same structure is chosen as for the pressure-based sensor we obtain

$$\beta_{i,j}^{\xi} = \frac{|\rho_{i+1,j} - 2\rho_{i,j} + \rho_{i-1,j}|}{(1-\chi)(|\rho_{i+1,j} - \rho_{i,j}| + |\rho_{i,j} - \rho_{i-1,j}|) + \chi(\rho_{i+1,j} + 2\rho_{i,j} + \rho_{i-1,j})} \tag{18}$$

and

$$\gamma_{i,j}^k = B^k \max(\beta_{i,j}^{\xi}, \beta_{i-1,j}^{\xi}, \beta_{i+1,j}^{\xi}, \beta_{i,j}^{\eta}, \beta_{i,j-1}^{\eta}, \beta_{i,j+1}^{\eta}) \tag{19}$$

The disadvantage of this sensor is that it is already activated in non-reactive flows if there are strong density gradients, e.g. in a shear flow with streams of different densities. For this reason Equation (16) is preferred and used throughout this paper. Two disadvantages are associated with any damping of the restricted residual error:

- the possible acceleration of the multigrid method is reduced in regions where damping is performed,
- and empirical constants (C^k or B^k) are required that may change from test case to test case.

Practical investigations have shown that the influence of the model constants is not very strong as long as the required minimum damping is exceeded. Moreover, a local damping still allows the full multigrid to work away from the small regions of combustion and shock waves. In case of damping the restricted residual error Hackbusch [21] proposed a corresponding amplification during prolongation. This did not work for the test cases investigated.

3.1.4. Highly stretched grids. The success of multigrid techniques in case of highly stretched grids depends on the kind of grid coarsening and the damping properties of the solver. For 2D simulations the implicit LU-SGS algorithm was found to sufficiently damp out high frequency error components even in case of high cell aspect ratio grids. For 3D simulations we use a semi-coarsening to avoid such problems.

4. RESULTS AND DISCUSSION

Several test cases have been calculated to investigate the convergence acceleration of the described multigrid scheme and to demonstrate the accuracy of the numerical method for the simulation of detached shock waves. While the first series of simulations treats non-reactive

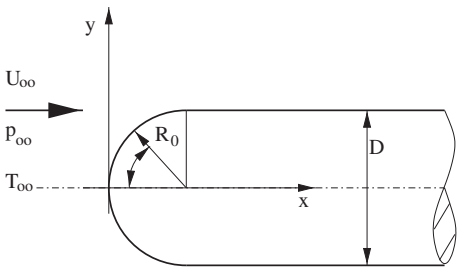

Figure 1. Geometry of the hemisphere cylinder.

Table I. Inflow conditions for supersonic and hypersonic flows over a hemisphere cylinder.

Test case	1	2	3	4	5	6
Ma	1.99	3.00	4.03	5.06	6.03	8.10
p (bar)	0.07139	0.06065	0.02909	0.01830	0.00740	0.00424
T (K)	171.3	120.0	81.5	59.5	49.6	52.7

air flows, the second test case additionally includes hydrogen combustion. In both cases results are compared with experimental data.

4.1. Non-reactive flows over a hemisphere cylinder

In case of supersonic and hypersonic flows over spheres or blunt shapes bow shocks are formed. As described before different detachment distances at different grid level may cause divergence of multigrid solvers. A series of multigrid simulations has been performed for the experiment of Baer [22]. The Mach numbers of these experiments and simulations are 2, 3, 4, 5, 6 and 8, and the Reynolds numbers vary between 6.69×10^6 and 2.01×10^7/m. Figure 1 shows a sketch of the model geometry, a cylinder with a spherical nose. The diameter of the cylinder is $D=147.32$ mm and wall pressures have measures up to $x=920$ mm. Inflow Mach numbers, static pressures and temperatures are summarized in Table I for the six different test cases. The uncertainty of the pressure measurements is reported to increase from $\pm1\%$ relative error for the Mach 2 case to $\pm5\%$ for the Mach 8 case based on repeatability of measurements [22]. All computational grids consist out of 1 block with 144×384 volumes. The grid is refined in the shock wave regions and near solid walls.

Schlieren photographs have been used to define the experimental shock position. Figures 2 and 3 show calculated pressure distributions for the Mach 2 and 6 flow, respectively (for Mach 8 no experimental shock position data is available). The experimentally obtained shock position is given by circles plotted in these figures. For all test cases there is a good agreement between simulation and experiment. Figure 4 shows a comparison between the normalized experimental and numerical wall static pressures along the spherical part of the model. Pressure profiles are plotted for all test cases versus the angle θ of the sphere. While results of the simulations are drawn with different types of lines symbols indicate experimental results. In Figure 5 the corresponding pressure distributions are plotted in the same way for the cylindrical part of the model. It may be observed that the agreement between

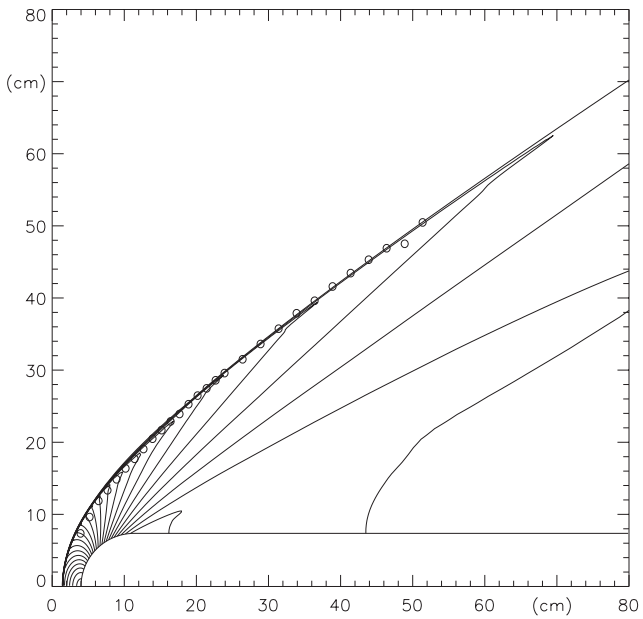

Figure 2. Calculated pressure contours and experimentally obtained shock position (○) for the Mach 2 test case.

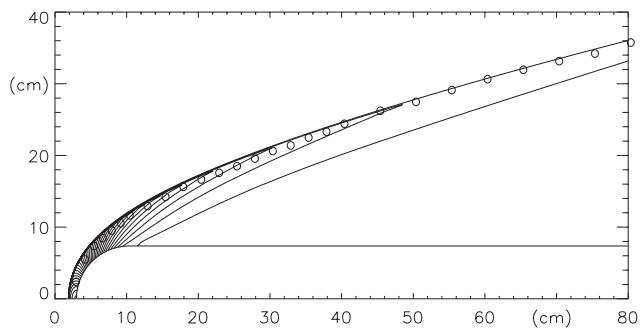

Figure 3. Calculated pressure contours and experimentally obtained shock position (○) for the Mach 6 test case.

simulation and experiment is very good for all experiments investigated. Finally, numerical and experimental shock wave detachment distances (at the symmetry axis) are given in Figure 6.

All test cases have been simulated with and without the multigrid technique. A full coarsening *V*-cycle multigrid method has been used with one iteration at every grid level. The nested iteration starts at the coarsest grid level to obtain good initializations of the flow field. Without damping of the restricted residual error near shock waves multigrid convergence was impossible. While the residual error damping was strictly required, the use of an upwind prolongation

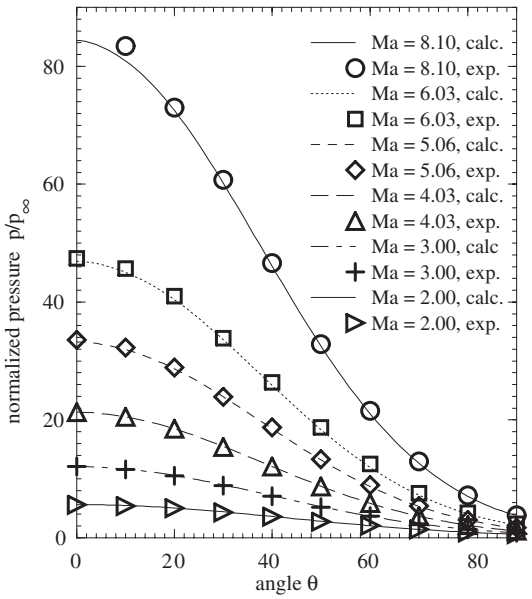

Figure 4. Calculated and experimentally obtained normalized wall static pressure versus sphere angle θ for Mach numbers 8, 6, 5, 4, 3, and 2.

technique [17] did not improve the convergence behaviour and therefore was not used in the following investigations. Figures 7 and 8 show the convergence histories of the averaged normalized density residual over the number of multigrid cycles and work units, respectively. One work unit corresponds to the computational time for one fine grid iteration. One full multigrid cycle requires about 2.47 times as much CPU time as one fine grid iteration. This is more than the theoretical possible value. One reason for this is that the simulations have been performed on a vector computer, a NEC SX-5. Due to shorter vector lengths especially in the implicit part of the LU-SGS algorithm on coarser meshes performance slows down. Thus on a scalar computer convergence acceleration due to the multigrid method should be slightly better. Convergence histories are given for the highest and lowest flow Mach numbers. After a first fast decrease of the residuals convergence slows down. In this part of the time integration the correct position for the bow shock wave has to be found. It may be observed that for the 1 and the 4 grid solution convergence improves with increasing Mach number. The most probable explanation for this effect is the decreasing detachment distance of the bow shock with increasing Mach number. The exact position of the bow shock is defined by aerodynamic reasons. If the detachment distance is smaller, finding this position is achieved faster by the numerical solver. As may be seen from Figure 6 the gradient of the detachment distance increases with decreasing Mach number. Thus, slight changes in the flow conditions cause strong changes in the bow shock position if the Mach number is low. The sensitivity of the bow shock position clearly decreases with increasing flight Mach number. This effect is reflected by the numerical simulation that require more iterations to find the correct shock position if the Mach number is low. Figure 8 shows a strong reduction of the required CPU time by the multigrid method. For a reduction of the residual by six orders in magnitude the

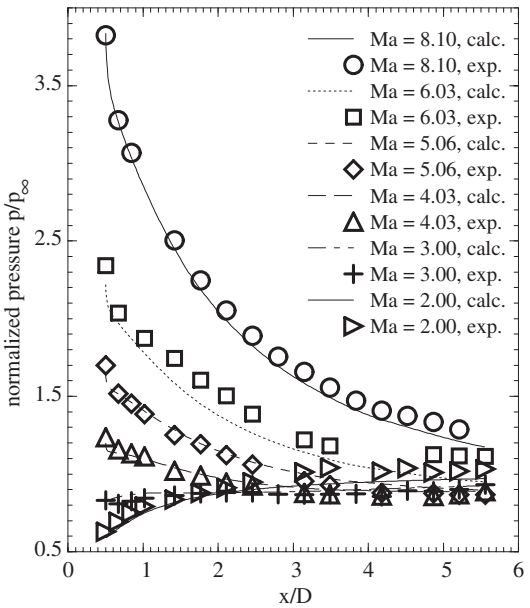

Figure 5. Calculated and experimentally obtained normalized wall static pressure versus normalized cylinder length for Mach numbers 8, 6, 5, 4, 3, and 2.

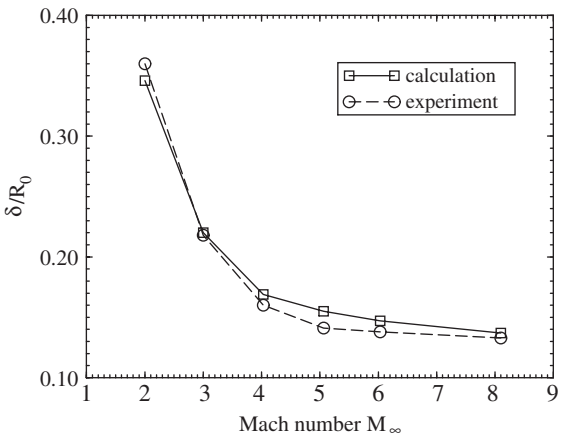

Figure 6. Calculated and experimentally obtained shock detachment distances at the symmetry axis versus Mach number.

multigrid technique requires only 20% of the one grid CPU time in case of the Mach 8 flow and 26% of the one grid CPU time for the Mach 2 flow. This is a significant acceleration. Moreover, the described changes in the multigrid technique to enable these accelerations work robust and are simple to implement.

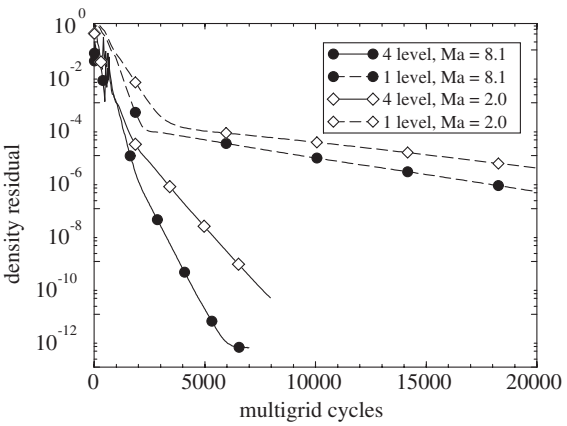

Figure 7. Convergence histories over the number of multigrid cycles with and without the multigrid technique for the Mach 2 and 8 test case.

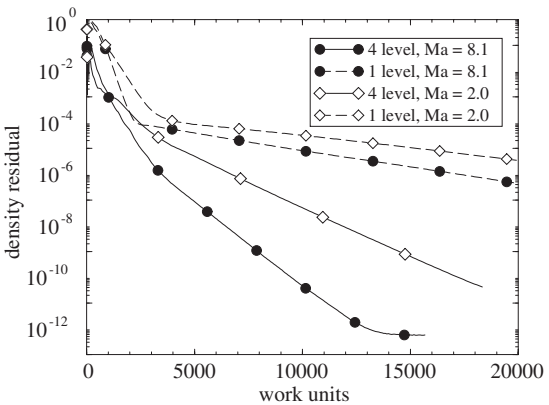

Figure 8. Convergence histories over the number of work units with and without the multigrid technique for the Mach 2 and 8 test case.

Next, the magnitude of the damping of the restricted residual error is investigated for the Mach 6 multigrid simulation. Figure 9 shows the damping coefficients during restriction from grid level 1 (finest grid) to 2 (upper figure), from grid level 2 to 3 (middle figure) and from grid level 3 to 4 (lower figure). Plotted are the terms $1 - \kappa^k$ used in Equation (15) to reduce the active coarse grid residuals. Due to the strong pressure gradients in the front part of the detached shock wave these damping coefficients are relatively low. This is in contrast to supersonic or hypersonic flows without normal shocks [7, 11, 13] where the required damping is much lower. We want to emphasize that these flows have been simulated with the same set of constants as oblique shock wave simulations. The stronger damping in case of normal or nearly normal shocks is a pure result of higher pressure ratios. Figure 9 demonstrates that the damping (with exception of the coarsest mesh) is limited to the direct vicinity of the shock

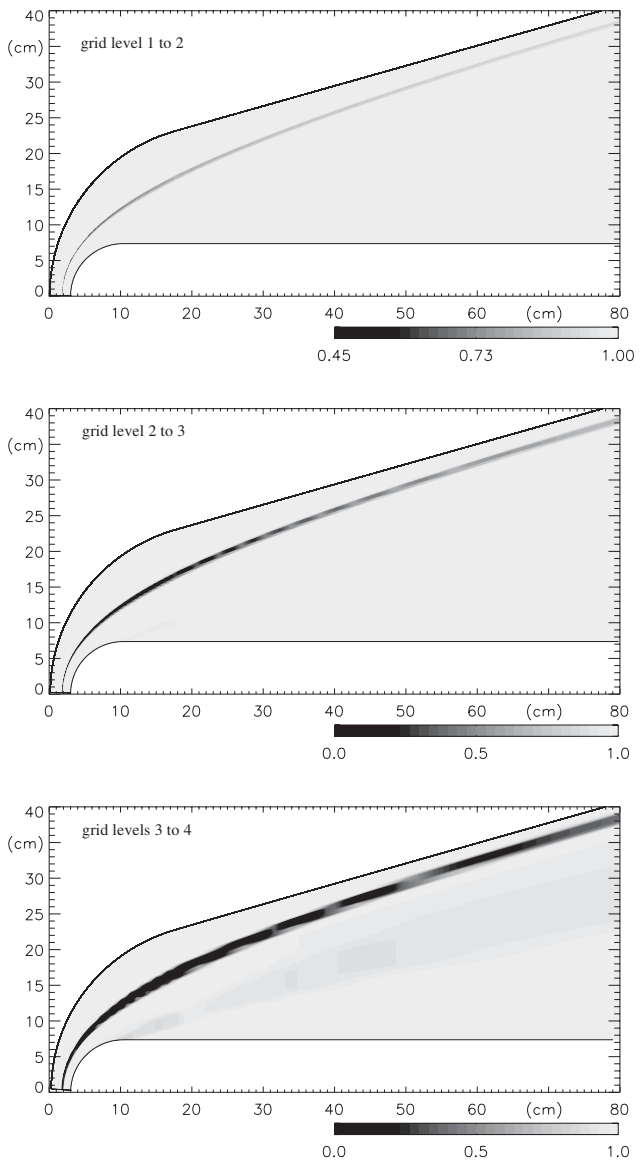

Figure 9. Pressure-based damping coefficients for the restriction of the residual errors from grid level 1 to 2 (upper figure), 2 to 3 (middle figure) and 3 to 4 (lower figure).

wave. While for the transfer from grid level 1 to 2 at least 45% of the residual is restricted, there are parts at grid levels 3 and 4 where the complete residual error is damped. However this concerns only volumes in the front part of the sphere where the shock wave is normal or nearly normal. Nevertheless, some of the fine grid information is lost during restriction being the price for stabilizing the multigrid method.

4.2. *Shock-induced combustion*

The experiment of Lehr [23] has been selected to investigate the described multigrid technique in case of shock-induced combustion. A spherical projectile with a diameter of 15 mm is shot at supersonic speed into a stoichiometric hydrogen air mixture. A series of different experiments has been performed by Lehr, where the flow Mach number and gas mixture has been varied. For the calculated Mach 6.46 test case stationary conditions are obtained. Two distinguishing features have been observed by shadowgraphs in the experiment: a bow shock ahead of the projectile similar to the bow shocks of the previous test cases and a following energy release front. Both effects are close to pure discontinuities. The exact position of the energy release front depends on the ignition delay time of the premixed gas. Therefore, the region between bow shock and energy release front is called induction zone [24]. Due to finite-rate chemistry effects both phenomena are separated. The calculated size of the induction zone is influenced by the reaction mechanism used. Different reaction mechanisms have been investigated for the simulation of this test case. Astonishingly, the best results where obtained by a relatively small reaction scheme with seven different species (N_2, O_2, H_2, H_2O, OH, O, and H) and seven reactions only [25]. Some larger and usually more accurate reaction schemes resulted in instationary behaviour and failure of the simulation. The same effect was observed by other researchers too [26]. Because the emphasis of the present paper is on the use of multigrid methods for detached shock waves, the influence of the different reaction mechanisms is not investigated any further.

Figures 10 and 11 show calculated pressure and density contours for the described test case. Pressure and temperature in front of the bow shock are 42 663 Pa and 292 K, respectively. The computational grid consists out of 128×144 volumes. As may be seen from the pressure distribution plotted in Figure 10 the simulated and experimental shock position (indicated by dark points) are in a very good agreement. Because the pressure remains constant over the energy release front it may not be visible in this figure. Density contours are chosen (see Figure 11) to indicate where the energy release front separates from the bow shock. Beside

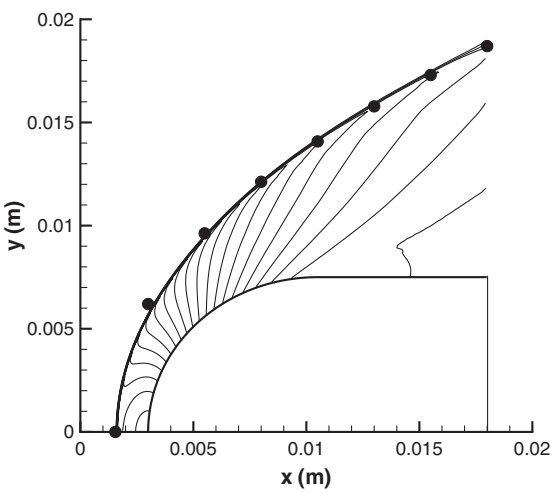

Figure 10. Calculated pressure contours and experimentally obtained shock position (•).

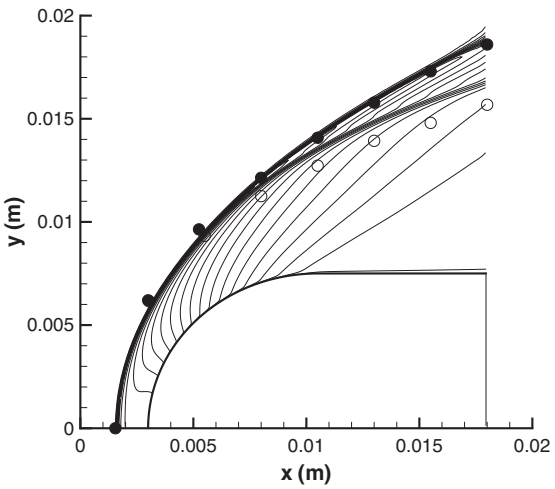

Figure 11. Calculated density contours, experimentally obtained shock position (●), and energy release front (○).

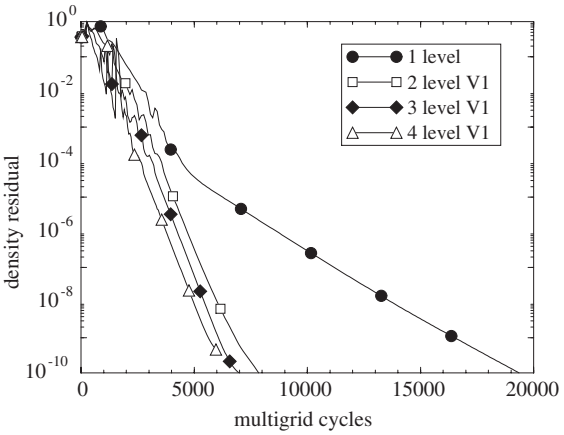

Figure 12. Convergence histories over the number of multigrid cycles with (2–4 grid levels) and without the multigrid technique.

the dark points showing the experimental shock position, the location of the energy release front is given by circles. The obtained ignition delay time of the simulation is shorter than in the experiment, clearly an effect of the reaction mechanism used. Nevertheless, the separating of bow shock and energy release front is clearly visible. Convergence histories for simulations with and without the nested multigrid technique are plotted in Figures 12 and 13. In contrast to the previous test case the one grid solution does not slow down as much as before with ongoing iteration. This may be due to the smaller size of the projectile, due to a smaller computational grid and due to the relatively simple flow structure. On the other hand, the convergence rates with multigrid technique are worse than for the non-reactive test case. In

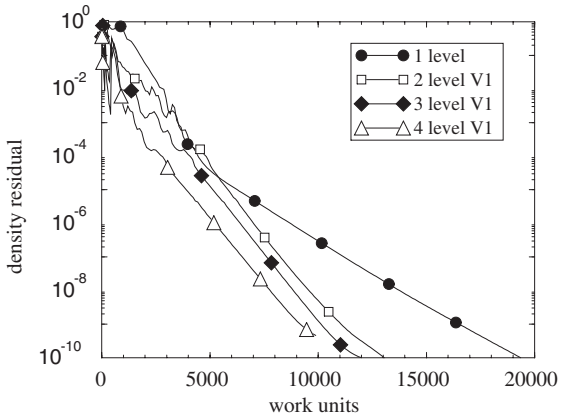

Figure 13. Convergence histories over the number of work units with (2–4 grid levels) and without the multigrid technique.

terms of CPU time reduction the benefit is smaller. By using the 4 level $V1$ multigrid method the required CPU time is about 55% of the one grid CPU time for a residual drop of eight orders in magnitude. To enable convergence slightly higher values for C^k had to be chosen than for the non-reactive test case. Thus in comparison to a two grid multigrid solution a third and fourth grid level achieved small improvements only. This simulation is close to a worst case for the multigrid technique described, because a detached shock wave with strong pressure gradients and a detached flame occurs. Moreover, the critical regions where damping has to be performed covers most of the features of the total flow field. Therefore, the test case also demonstrates the limitations of the described damping. On the other hand, even for this simulation multigrid convergence is possible and the required CPU time of 4 level multigrid solution is nearly half the CPU time of the single grid solution (on a vector computer). Thus even under unfavourable conditions considerable accelerations are possible. Especially, the simplicity of this technique makes it attractive to many multigrid users.

5. CONCLUSIONS

A modified multigrid method has been used successfully for the simulation of detached shock waves over a wide range of Mach numbers. In these cases multigrid convergence is enabled by a local damping of the restricted residual error in the vicinity of shock waves. Due to higher sensitivities of the bow shock position at low supersonic speed the convergence rates increase with increasing Mach number for single and multigrid simulations. For the non-reactive test cases the required CPU time is reduced up to 20% of the single grid CPU time. For the premixed reactive flow field with shock-induced combustion the required multigrid CPU time is about 55% of the single grid CPU time. This is less than convergence accelerations achieved for attached shock waves and attached flames. Because the location of detached shock waves is defined by aerodynamic reasons and that of a detached flame by kinetic reasons there may be a shift in bow shock or flame position at different grid levels. This requires a stronger damping for multigrid method to converge and reduces the possible amount of convergence

acceleration. Nevertheless, a considerable reduction in CPU time is achieved by this technique. It is simple to implement and works robust and reliable in supersonic and hypersonic flow.

ACKNOWLEDGEMENTS

We wish to thank the Deutsche Forschungsgemeinschaft (DFG) for the financial support of this work within the collaborative research center SFB 259 at the University of Stuttgart.

REFERENCES

1. Brandt A. Barriers to achieving textbook multigrid efficiency (TME) in CFD. *ICASE Interim Report No. 32*, NASA/CR-1998-207647, 1998.
2. Brandt A, Yavneh I. On multigrid solutions of high-Reynolds incompressible entering flows. *Journal of Computational Physics* 1992; **101**:151–164.
3. Roberts T, Sidilkover D, Swanson RC. Textbook multigrid efficiency for the steady Euler equations. *AIAA Paper 97-1949*, 1997.
4. Thomas JL, Bonhaus DL, Anderson WK, Rumsey CL, Biedron RT. An $O(Nm^2)$ plane solver for the compressible Navier–Stokes equations. *AIAA Paper 99-0785*, 1999.
5. Brandt A, Diskin B, Thomas JL. Recent advances in achieving textbook multigrid efficiency for computational fluid dynamics simulations. *ICASE Report No. 2002-16*, NASA/CR-2002-211656, 2002.
6. Edwards JR. Advanced implicit algorithms for finite rate hydrogen-air combustion calculations. *AIAA Paper 96-3129*, 1996.
7. Gerlinger P, Stoll P, Brüggemann D. An implicit multigrid method for the simulation of chemically reacting flows. *Journal of Computational Physics* 1998; **146**:322–345.
8. Gerlinger P, Möbus H, Brüggemann D. An implicit multigrid method for turbulent combustion. *Journal of Computational Physics* 2001; **167**:247–276.
9. Brandt A. Multi-level adaptive solutions to boundary-value problems. *Mathematics of Computation* 1977; **31**:333–390.
10. Brandt A. Multi-level adaptive solutions in fluid dynamics. *INKA-Conference-79*, *351-010*, *79-1455*, 1979.
11. Jameson A, Yoon S. Lower–upper implicit schemes with multiple grids for the Euler equations. *AIAA Journal* 1987; **25**:929–935.
12. Gerlinger P, Stoll P, Brüggemann D. A robust implicit multigrid method for the simulation of turbulent supersonic mixing. *AIAA Journal* 1999; **37**:766–768.
13. Gerlinger P, Brüggemann D. Multigrid convergence acceleration for turbulent supersonic flows. *International Journal for Numerical Methods in Fluids* 1997; **24**:1019–1035.
14. Koren B, Hemker PW. Damped, direction-dependent multigrid for hypersonic flow computations. *Applies Numerical Mathematics* 1991; **7**:309–328.
15. Coakley TJ, Huang PG. Turbulence modelling for high speed flows. *AIAA Paper 92-0436*, 1992.
16. Shuen JS. Upwind differencing and LU factorization for chemical non-equilibrium Navier–Stokes equations. *Journal of Computational Physics* 1992; **99**:233–250.
17. Gerlinger P, Algermissen J, Brüggemann D. Matrix dissipation for central difference schemes with combustion. *AIAA Journal* 1999; **33**:1865–1870.
18. Leclercq MP, Stoufflet B. Characteristic multigrid method application to solve the Euler equations with unstructured and unnested grids. *Journal of Computational Physics* 1993; **104**:329–346.
19. Ferm L, Lötstedt P. Two-grid solutions of shock waves. *SIAM Journal on Scientific Computing* 1997; **18**: 1533–1552.
20. Radespiel R, Swanson RC. Progress with multigrid schemes for hypersonic flow problems. *Journal of Computational Physics* 1995; **116**:103–122.
21. Hackbusch W. *Multigrid Methods and Applications*. Springer: Berlin, 1985.
22. Baer AL. Pressure distributions on a hemisphere cylinder at supersonic and hypersonic Mach numbers. *AEDC-TN-61-96*, 1961.
23. Lehr HF. Experiments on shock induced combustion. *Astronautica Acta* 1972; **17**:589–597.
24. Wilson GJ, Sussman MA. Computation of unsteady shock-induced combustion using logarithmic conservation equations. *AIAA Journal* 1993; **31**:294–301.
25. Drummond JP, Rogers RC, Hussaini MY. A detailed numerical model of a supersonic reacting mixing layer. *AIAA Paper 86-1427*, 1986.
26. Clutter K, Krishnamurty V, Shyy W. Combustion and turbulence effects in hypersonic projectile flows. *AIAA Paper 97-0807*, 1997.

